7-19-2022

Activation domains can decouple the mean and noise of gene expression

Kaiser Loell
Washington University School of Medicine in St. Louis
Yawei Wu
Washington University School of Medicine in St. Louis
Max V Staller
University of California - Berkeley
Barak Cohen
Washington University School of Medicine in St. Louis

Cell Reports

Activation domains can decouple the mean and noise of gene expression

Graphical abstract

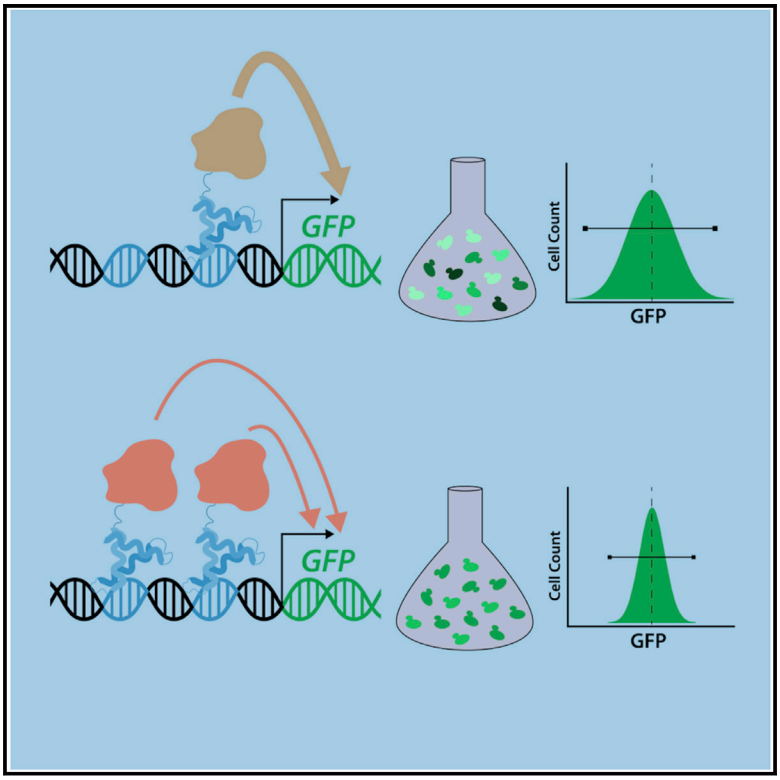

Highlights

- Orthogonal perturbations to TF AD and level can decouple mean and noise
- Differences in noise can be explained solely in terms of TF occupancy and AD potency
- The random telegraph model explains observed mean-noise relationships
- TF level affects multiple parameters, while AD potency primarily affects burst size/Km

Authors

Kaiser Loell, Yawei Wu, Max V. Staller, Barak Cohen

Correspondence

cohen@wustl.edu

In brief

Gene expression varies widely, even in populations of otherwise identical cells. Loell et al. show that the degree of variation ("noise") can be controlled independently of the average level of expression ("mean") by simultaneously varying a transcription factor's activation domain (AD) and the amount of it in the nucleus.

Loell et al., 2022, Cell Reports *40*, 111118
July 19, 2022
https://doi.org/10.1016/j.celrep.2022.111118

CellPress

Cell Reports

CellPress
OPEN ACCESS

Report

Activation domains can decouple the mean and noise of gene expression

Kaiser Loell,[1,2] Yawei Wu,[1,2] Max V. Staller,[3] and Barak Cohen[1,2,4,*]
[1]Department of Genetics, Washington University School of Medicine in St. Louis, St. Louis, MO 63108, USA
[2]The Edison Family Center for Genome Sciences & Systems Biology, Washington University School of Medicine in St. Louis, St. Louis, MO 63108, USA
[3]Center for Computational Biology, University of California, Berkeley, Berkeley, CA 94720, USA
[4]Lead contact
*Correspondence: cohen@wustl.edu
https://doi.org/10.1016/j.celrep.2022.111118

SUMMARY

Regulatory mechanisms set a gene's average level of expression, but a gene's expression constantly fluctuates around that average. These stochastic fluctuations, or expression noise, play a role in cell-fate transitions, bet hedging in microbes, and the development of chemotherapeutic resistance in cancer. An outstanding question is what regulatory mechanisms contribute to noise. Here, we demonstrate that, for a fixed mean level of expression, strong activation domains (ADs) at low abundance produce high expression noise, while weak ADs at high abundance generate lower expression noise. We conclude that differences in noise can be explained by the interplay between a TF's nuclear concentration and the strength of its AD's effect on mean expression, without invoking differences between classes of ADs. These results raise the possibility of engineering gene expression noise independently of mean levels in synthetic biology contexts and provide a potential mechanism for natural selection to tune the noisiness of gene expression.

INTRODUCTION

Gene expression is an inherently stochastic process, producing levels of protein and mRNA that fluctuate between genetically identical cells (Elowitz et al., 2002; Raj et al., 2006; Shahrezaei and Swain, 2008a, 2008b; Kepler and Elston, 2001). This stochasticity, or noise, in gene expression is unavoidable due to the randomness of molecular motions. Noise is a fundamental property of gene expression with phenotypic consequences that have been observed across all domains of life and scales of organization (Raj and Van Oudenaarden, 2008; Gandrillon et al., 2012).

Stochastic noise in gene expression tends to occur in bursts during which many mRNAs are transcribed within a short period, interspersed within longer silent intervals (Paré et al., 2009; Singh et al., 2010; Halpern et al., 2015; Chubb and Liverpool, 2010; Dar et al., 2012, 2016; Tantale et al., 2016). This bursty gene expression has been observed in bacteria (Golding et al., 2005), yeast (Zenklusen et al., 2008), and mammalian cells (Halpern et al., 2015). One major consequence of bursty gene expression noise is its effect on cell fate decisions (Symmons and Raj, 2016; Balázsi et al., 2011; Losick and Desplan, 2008; Bell et al., 2007), which are frequently determined by stochastic fluctuations in the levels of transcriptional regulators (Miller et al., 2008; Chang et al., 2008; Pina et al., 2012; Graf and Enver, 2009; Enver et al., 2009; Cross and Enver, 1997; Wolff et al., 2018; van Roon et al., 1989; Fiering et al., 1990; Dingemanse et al., 1994; Walters et al., 1995). Stochasticity in cell fate decisions represents a "bet hedging" strategy that keeps cellular phenotypes diverse, even in the absence of genetic or environmental variation (Rouzine et al., 2015; Singh and Weinberger, 2009; Weinberger et al., 2005, 2008; Schwall et al., 2021; St-Pierre and Endy, 2008; Zeng et al., 2010; Golding, 2011; Dar et al., 2014; Razooky et al., 2015).

Efforts to understand the molecular causes of expression noise have shown that both *cis* (Raser and O'Shea, 2004; Walters et al., 1995; Anderson et al., 2017; Waymack et al., 2020) and *trans* factors (Ahmad and Henikoff, 2001; Hensel et al., 2012; Kalo et al., 2015; Kafri et al., 2016) influence noise in gene expression. Transcription factors (TFs) are a known source of expression noise (Senecal et al., 2014). TFs are composed of DNA binding domains, which confer specificity for their target CREs, and activation domains (ADs), which recruit *trans*-acting cofactors that alter transcription once bound to DNA (Näär et al., 2001; Govind et al., 2005). Fluctuations in TF binding are a major determinant of gene expression noise (Parab et al., 2021; Senecal et al., 2014; Pelet et al., 2011), but the effects of TF ADs on expression noise have not been determined. Because ADs vary widely in the cofactors they recruit and the contexts in which they are active (Blau et al., 1996; Brown et al., 1998; Duarte et al., 2016; Stampfel et al., 2015), we investigated whether ADs also vary in their effects on noise in gene expression.

Two hypotheses might explain how ADs influence noise in gene expression. One hypothesis is that the noise generated by an AD depends solely on its effect on mean levels of

expression. Noise is tightly coupled to mean output levels in most stochastic processes (Vallania et al., 2014). Thus, increasing a gene's mean expression necessarily increases its expression noise. This hypothesis is consistent with the increase in noise produced by VP64 relative to VP16 (Senecal et al., 2014). A strong prediction of this hypothesis is that diverse ADs will all generate the same amount of noise for a given mean level of expression. An alternate hypothesis is that an AD's effect on noise depends both on its effect on mean expression and on the specific cofactors that underpin its activity. Different ADs might produce different amounts of noise, even at the same mean output level, because of the distinct biochemical properties of the cofactors they recruit. For example, it has been suggested (Pelet et al., 2011) that recruitment of chromatin remodelers is a key step in generating gene expression variation. If this is the case, TFs with activation domains that recruit chromatin remodelers will have distinctly different effects on noise from those that cannot. This hypothesis is supported by Tan et al.'s observations of the effects on noise of mutations in the p65 AD that ablate binding to CBP/p300 (Tan et al., 2021). However, because only a very limited number of ADs have been tested, it remains unresolved which hypothesis applies more generally.

RESULTS

A reporter system that measures the effects of different ADs on expression noise

To compare the effects of diverse ADs on expression noise, we set up a reporter system that allowed us to measure the mean and noise of expression generated by TFs that differ only in the AD they carry. We repurposed the reporter system described in Staller et al. (2018); Figure 1A), which uses synthetic *S. cerevisiae* TFs consisting of an AD of interest, a fluorescent tag (mCherry), an estrogen response domain (ERD), and a fixed synthetic zinc-finger DNA binding domain (DBD) (McIsaac et al., 2013). Using a synthetic DBD avoids interference with endogenous yeast TFs, and the ERD allows us to control the nuclear localization of the synthetic TFs with β-estradiol. Swapping the ADs on these synthetic TFs allowed us to directly compare the effects of different ADs while keeping the rest of the TF constant and avoiding competition with endogenous TFs.

We measured the activities of these synthetic TFs by reading out the fluorescence of a GFP reporter construct via flow cytometry. The reporter construct contains a tandem array of zinc-finger binding sites and is integrated at a single allele of the *URA3* locus. To probe the impact of varying TF stimulation on target expression, we performed dose-response experiments with increasing amounts of β-estradiol and measured the resulting distribution of GFP by flow cytometry. We did not observe any effect on cell growth from the β-estradiol, either in the side and forward scatter measurements (Figure S1A) or in the growth rates (Figure S2). We then computed the mean (x) and Fano factor (σ^2/x) of expression for each TF at each β-estradiol concentration. We used the Fano factor as the measure of noise because it normalizes for different mean levels of expression (Blake et al., 2003; Munsky et al., 2012; Ozbudak et al., 2002; Sanchez and Golding, 2013).

A gene's expression noise can be divided into an intrinsic and extrinsic component (Swain et al., 2002). We focused on the effect of ADs on the intrinsic component because current models of stochastic gene expression best capture intrinsic noise. We therefore attempted to exclude extrinsic noise from our measurements.

The presence of significant extrinsic noise in our data was indicated by a strong correlation between the forward scatter, side scatter, GFP, and mCherry fluorescence in the raw data. However, after controlling for cell size by gating on forward scatter, there was little correlation between the expression of the TF construct as measured by mCherry signal and GFP expression (Figure S1B). We speculate that there is no residual correlation between mCherry and GFP because of the time lag between the production of mCherry-tagged TFs and the expression and maturation of the GFP reporter or because the mCherry signal reflects the TF concentration throughout the cell and is not specific for the nucleus.

To screen out this source of extrinsic noise, we filtered our data by gating on cells expressing similar levels of mCherry, which removed 56% of the total variance in GFP expression. We chose mCherry as the marker to filter by to exclude a small (<1%) outlier subpopulation of events with similar scatter to most cells but very high mCherry and low GFP. While filtering on mCherry does not exclude all extrinsic noise related to forward scatter, additional filtering on forward scatter leaves few cells, which lowered reproducibility without affecting the overall shape of the mean-Fano relationships. Using this system, we compared the effects of diverse ADs on both the mean and noise of expression.

Comparison of the VP16 and Gcn4 ADs demonstrates that it is possible to decouple expression noise from the mean

We first compared the effects of a strong AD (VP16) and a weak AD (Gcn4) on expression mean and noise by performing dose-response experiments. Varying the levels of induction for each synthetic TF led to Fano factors increasing with mean reporter protein expression. Strikingly, VP16 produced more gene expression noise than Gcn4 for every mean level of reporter expression tested (Figure 1B). This result indicates that different ADs can create different amounts of noise in gene expression, even when the mean expression level is the same.

Because the VP16 AD is stronger than the Gcn4 AD, the Gcn4 construct always required higher β-estradiol concentrations than VP16 to achieve the same mean reporter expression level. This observation led us to a working hypothesis that high expression noise is produced by strong ADs present at low nuclear concentrations, whereas low expression noise is achieved by weak ADs present at high nuclear concentrations.

Comparisons of multiple activation domains reveal that expression noise can be explained by AD strength

Our working hypothesis assumes that the noise generated by an AD is determined solely by its strength and nuclear concentration. Alternatively, different ADs might generate different amounts of noise based on the distinct cofactors they recruit. These two possibilities can be distinguished by measuring the

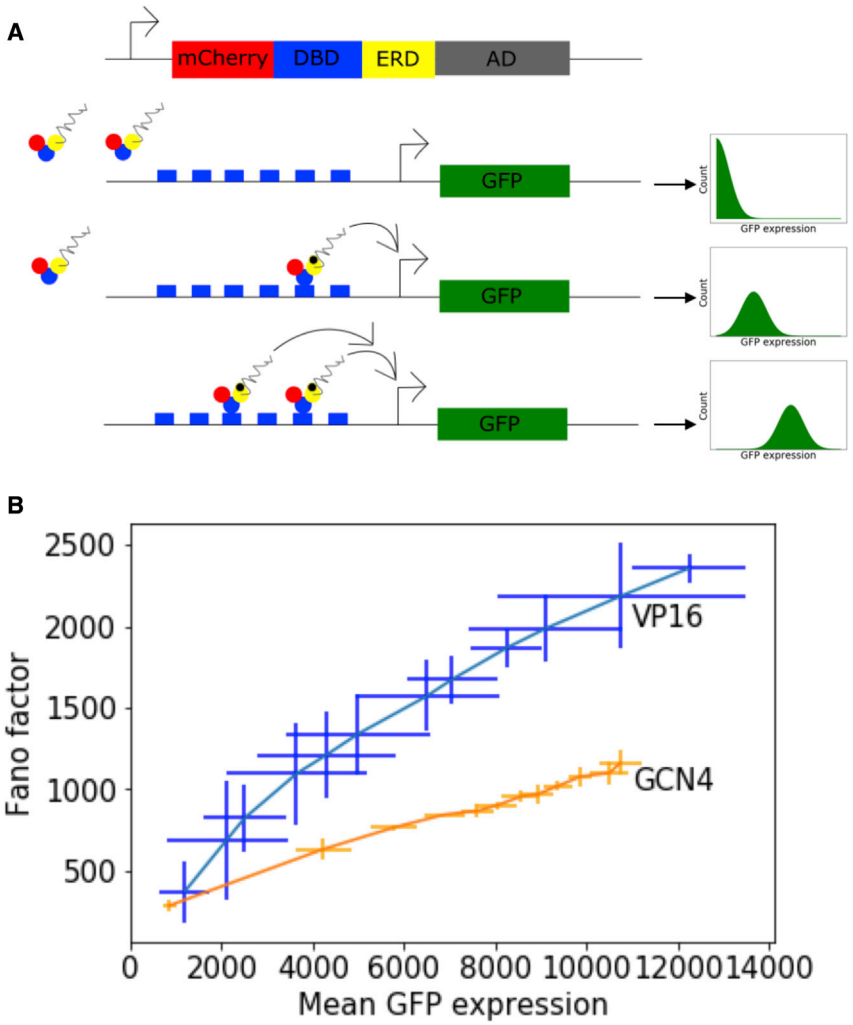

Figure 1. Comparison of the VP16 and Gcn4 ADs

(A) Reporter system to measure the mean and noise produced by diverse ADs. Synthetic TF constructs are composed of an mCherry tag (red), a fixed zinc-finger DBD (blue), an estrogen response domain (yellow), and a variable AD (gray). Synthetic TFs induce GFP expression (green) from a reporter gene driven by an array of zinc-finger binding sites. Varying levels of β-estradiol (black) control the nuclear localization of the synthetic TFs, allowing precise control of nuclear concentration while controlling for AD.

(B) Activation domains differ in the amount of noise they induce, even at comparable means. The noise (Fano factor) produced by synthetic TFs carrying either the Gcn4 or VP16 AD is plotted for varying mean levels of reporter gene expression. The trend lines connect the data points and are not model fits to the data. Error bars are standard deviations over three replicates.

mean and noise induced by a diverse set of ADs at the same β-estradiol concentration. If the differences in noise were due only to differences in the strengths and nuclear concentrations of ADs, then, for a fixed level of induction, the noise generated by ADs would be predictable from the mean levels of reporter gene expression they produce. Alternatively, if certain ADs had special biochemical properties, then such ADs would deviate from the mean versus noise trendline.

To test these predictions, we assayed 11 different yeast ADs and a negative control at a fixed β-estradiol concentration. This experiment revealed a linear relationship between the mean and noise of expression for all ADs tested (Pearson R^2 = 0.90) (Figure 2A). We observed similar linear trends at different fixed β-estradiol concentrations (Figure S3J). To confirm that the AD does not affect the TF construct's localization, we imaged the subcellular localization of the TF construct using the mCherry tag. The ratio of nuclear to total mCherry fluorescence was distributed similarly across strains (Figure S4), indicating that the AD does not affect the TF's nuclear concentration. In the Saccharomyces Genome Database (https://www.yeastgenome.org/), most of the TFs from which these ADs derive interact with unique cofactors (examples in Figure S5), suggesting that they activate transcription through different mechanisms. Thus, at a fixed nuclear concentration, diverse ADs follow a predictable trend relating the mean and noise of expression they produce.

We next asked whether mutants that interfere with the mechanism of action of ADs alter the fixed relationship between the mean and noise produced by ADs. We assayed, at a fixed β-estradiol concentration, the activities of 84 mutants in the Gcn4 AD from Staller et al. (2018). This set was chosen to cover a broad range of mutation types and activities. Although the mutants produced a wide range of mean reporter gene activities, we still observed a strong linear relationship between the mean and noise of expression across all mutants (Pearson R^2 = 0.91) (Figure 2B).

Taken together, these results demonstrate that it is difficult to uncouple the mean and noise of expression at a fixed nuclear concentration of AD. At a fixed nuclear concentration, diverse ADs and a diverse set of AD mutants both exhibit a tight coupling between mean and noise. These observations support our working hypothesis that noise in gene expression is controlled by the interplay between the strength and nuclear concentration of ADs and not by the specific mechanism of action of ADs.

Simulations provide a mechanistic interpretation of the results

We asked what quantitative models of gene expression noise could explain the above observations and whether we could link perturbations of specific kinetic parameters of those models to the observed effects of perturbing AD strength or nuclear concentration.

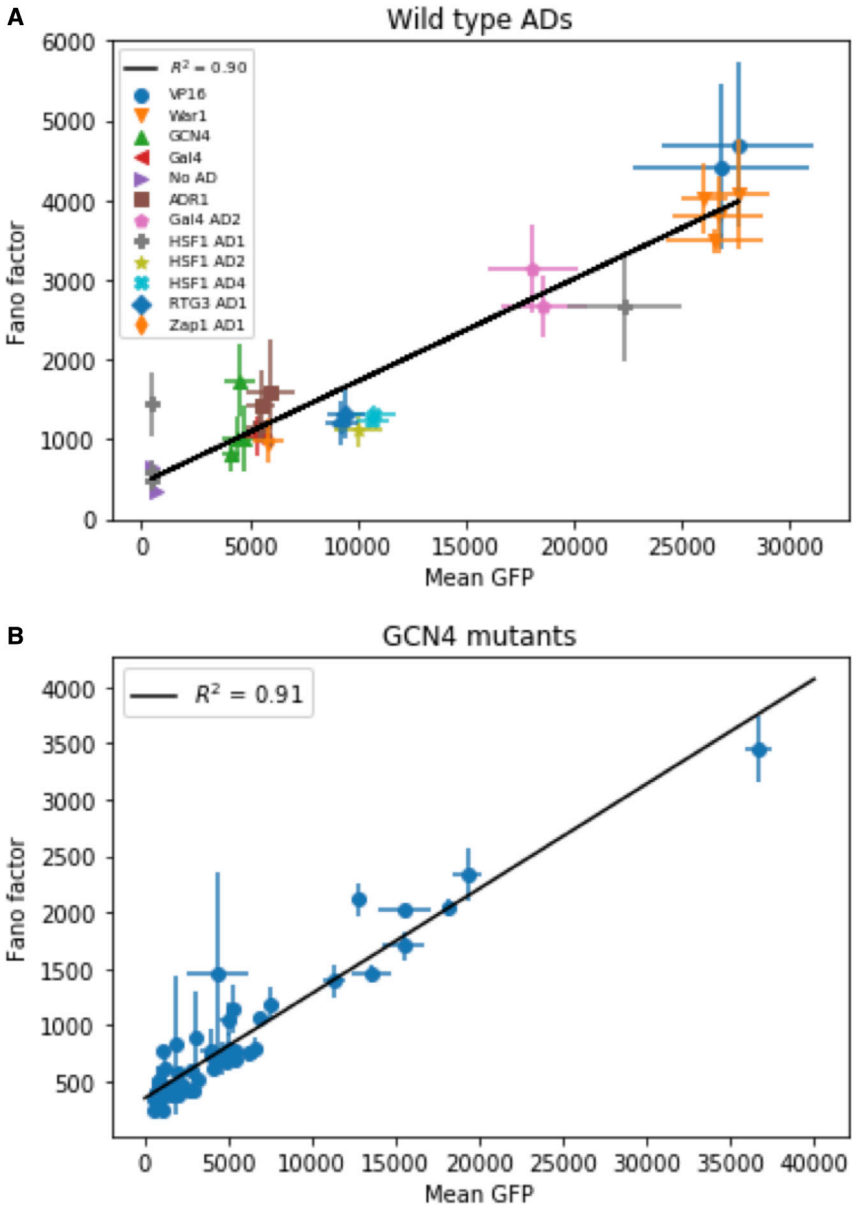

Figure 2. Comparisons of multiple activation domains

(A) Linear relationship between activation domain strength and noise for diverse ADs. The noise produced by diverse ADs is plotted versus the mean level of reporter gene expression for each AD. Error bars are standard deviations of mean and Fano across three replicates.

(B) Linear relationship between activation domain strength and noise for mutants in the Gcn4 AD. The noise produced by each Gcn4 AD mutant is plotted versus its mean reporter gene expression. Error bars are standard deviations over three replicates.

To identify perturbations that could reproduce the effects of varying the nuclear concentrations of ADs, we aimed to identify single parameters or linearly related pairs of parameters that, when varied, reproduced our experimental observations. We performed simulations in which we varied one or two parameters in the model through its physiological range while holding the other parameters in the model at fixed values. We performed these simulations many times, each time holding the other parameters in the models at different fixed values. We found no individual parameter that when varied reproduced our experimental observation that the Fano factor-mean relationship is nonlinear with a decreasing slope. However, linear perturbations to two parameters simultaneously could recapitulate the experimental effects of increasing nuclear concentration (Figure S6). More specifically, we found that, assuming the random telegraph model (Shahrezaei and Swain, 2008a, 2008b; Sherman and Cohen, 2014; Tiberi et al., 2018; Figure 3A), increasing K_{on} (the frequency of transitioning to the active state) while simultaneously increasing K_m (the transcription rate while in the active state) (Figure 3E) or decreasing D_m (the mRNA degradation rate) (Figure 3F) produced trendlines that resembled those associated with increasing nuclear concentration of TF.

All other models we tested either could not explain our observations or provided no additional explanatory value. The mean-noise relationships predicted by the transcription cycle model (Scholes et al., 2017; Figure 3B) sharply contrast with those we observe. Altering either parameter of this model is predicted to cause Fano factor to fall then rise with mean (Figures S6G–S6I). Simulations performed across a range of combinations of parameters predicted that noise would be at a minimum when the two rates are equal, with noise increasing with increasing disparity between the parameters. The refractory period model's (Zoller et al., 2015; Figure 3C) predictions also conflict with our observations. This model predicts two qualitatively distinguishable mean-Fano factor relationships, with changes in the rates of steps leading out of the active state causing Fano factor to change linearly with mean (Figures S6O and S6P) and changes in the remaining steps having no effect on noise (Figures S6J–S6N).

The effects of varying the AD strength were more straightforward to recreate in models. Again, assuming the random telegraph model, linear increases in K_m, with or without concurrent changes in D_m, produced linear mean-Fano relationships matching those we observed when AD strength is varied (Figures 3G and 3H). Sherman and Cohen's (Sherman and Cohen, 2014) analytical solution for the moments of the random telegraph model's protein distribution also predicted these mean-Fano relationships (Figures S6Q–S6S). Varying K_m while holding K_{on} or K_{off} fixed at different values produced different slopes but

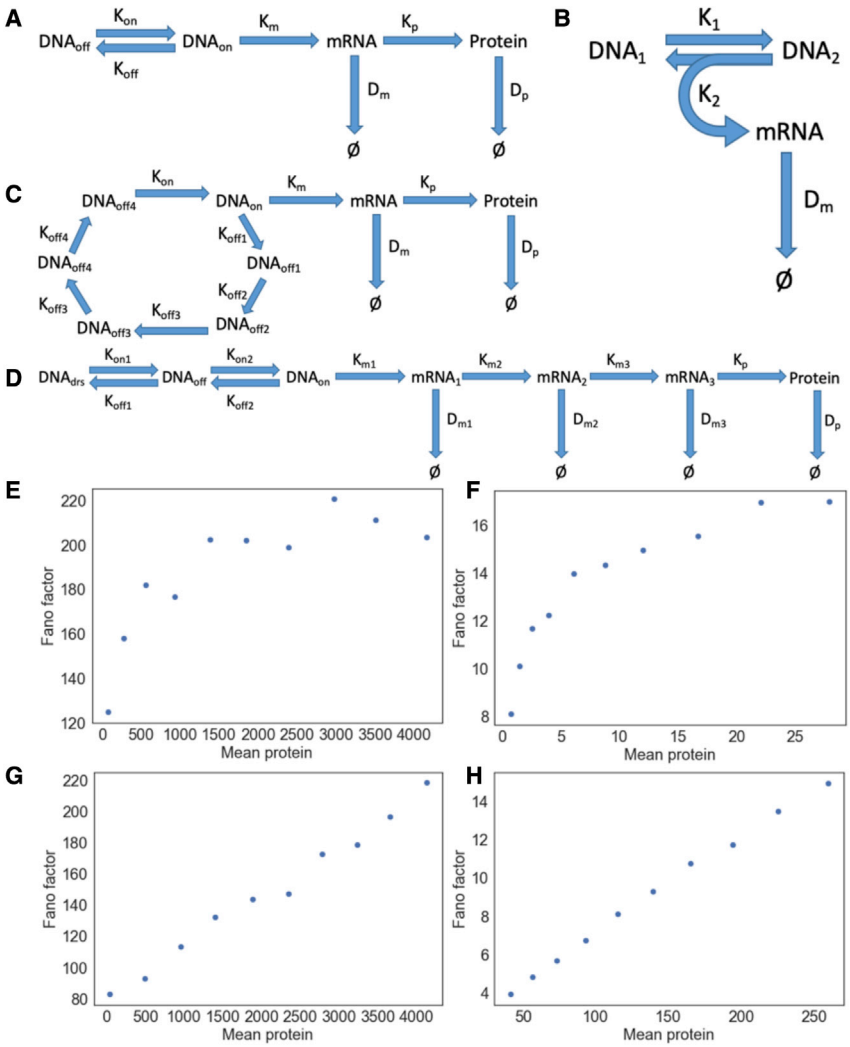

Figure 3. Stochastic models of gene expression

(A–D) Cartoon diagrams of (A) the random telegraph model, (B) the transcription cycle model of Scholes et al. (2017), (C) the refractory model of Zoller et al. (2015), and (D) the multi-state model of Rodriguez et al. (2019).

(E–H) The mean (x axis) and Fano factor (y axis) of protein expression predicted by the random telegraph model are plotted for simulations in which (E) K_{on} and K_m are varied simultaneously, (F) K_{on} and D_m are varied simultaneously, (G) K_m is varied, or (H) K_m and D_m are varied simultaneously.

otherwise preserved the linear mean-Fano relationship produced by ADs of increasing strength, whereas varying K_{on} or K_{off} could not reproduce this trend, regardless of the value of K_m (Figure S6).

The multi-state model (Rodriguez et al., 2019; Figure 3D), while able to reproduce our experimental results, did not fit our observations better than the less complex random telegraph model. It predicted mean-variance relationships similar to those of the random telegraph model, with modulating the rates of transition into and out of the long-lived repressed state predicted to have effects resembling those of modulating K_{off} (Figure S6T) and K_{on} (Figure S6U) in the random telegraph model, respectively, and changes in the rates of the other steps having effects (Figures S6V–S6X) similar to those of changes in K_m.

We conclude that the random telegraph model is the simplest model that captures the effects of both varying the strength and nuclear concentration of ADs. In addition, we conclude that the nuclear concentration of a TF influences K_{on}, while AD strength primarily acts through K_m. This can further be interpreted in terms of transcriptional burst parameters. K_{on} in the random telegraph model is effectively equivalent to burst frequency, while burst size is proportional to the ratio of K_m to K_{off}. We therefore conclude that AD strength primarily controls burst size, while the nuclear concentration of an AD affects burst frequency.

DISCUSSION

We demonstrate here that the mean and noise of gene expression can be separated by varying the strength and nuclear concentration of ADs. By varying the induction levels of different ADs, we observed noise levels spanning a roughly 2-fold range at comparable means. These results raise the possibility of synthetically manipulating expression mean and noise independently by using ADs of varying strength while tuning TF occupancy on DNA to compensate. Doing so would have many applications in synthetic biology, allowing perturbation experiments aimed at determining the effects of noise on gene expression networks, development, and cellular physiology and opening the way for engineering stochastic fate decisions during cellular reprogramming. Likewise, natural selection could tune the noisiness of a gene's expression, independent of its mean levels, by operating on variation that affects the strength and nuclear concentrations of ADs.

Our results can be explained in terms of the effects of AD strength and TF concentration in the nucleus. TF binding to DNA occurs for only brief periods (Normanno et al., 2015; Zhang et al., 2016; Liu and Tjian, 2018; Hansen et al., 2020), leading to intermittent transcriptional activation. At low TF concentrations, there is low TF occupancy on the DNA. Coupled with a strong AD, this regime leads to large but infrequent bursts of expression, which produce high noise. Conversely, at high TF concentrations, there is much higher promoter occupancy, leading to more frequent bursts approaching a continuous rate of mRNA production and therefore relatively low noise. Maintaining the same mean level of expression in this regime requires lowering the strength of the AD to compensate for more frequent bursting.

Our working hypothesis that both nuclear concentration and AD strength determine noise can be formulated quantitatively

in terms of the random telegraph model of gene expression kinetics. The components of the random telegraph model are both necessary and sufficient to explain our results: models such as Zoller et al.'s (Zoller et al., 2015)and Scholes et al.'s (Scholes et al., 2017)that cannot be reduced to the random telegraph model are unable to produce the mean-Fano relationships we observe experimentally, and those such as Rodriguez et al.'s (Rodriguez et al., 2019) that add additional steps to the random telegraph model do not provide additional explanatory power. Our results thus favor models without cycles or refractory states as the more parsimonious explanation.

Based on the simulation and experimental results, we posit that AD strength primarily affects K_m, the rate of transcription from the promoter in its active state, while the abundance of TF in the nucleus determines K_{on}, the rate at which the promoter switches into the transcriptionally active state. Under these assumptions, the random telegraph model predicts mean-Fano factor relationships resembling those we observed experimentally. Future work will elucidate the role of DBD affinity for sequence motifs, cooperative TF binding, and other *cis* factors in TF regulation of transcriptional noise.

Limitations of this study

Synthetic TFs were used throughout this study. Their use is necessary to control for DNA binding and isolate the effects of AD sequences and nuclear concentration but could, in theory, alter the properties of the ADs from their physiological context. In addition, we performed all experiments in yeast because it is a highly tractable model system. Because of this, the generalizability of our results to mammalian contexts depends on the conservation of transcriptional regulatory mechanisms across eukaryotes.

STAR★METHODS

Detailed methods are provided in the online version of this paper and include the following:

- KEY RESOURCES TABLE
- RESOURCE AVAILABILITY
  - Lead contact
  - Materials availability
  - Data and code availability
- EXPERIMENTAL MODEL AND SUBJECT DETAILS
  - Yeast strains
  - Culture conditions
- METHOD DETAILS
  - Molecular cloning and transformations
  - Beta-estradiol induction and flow cytometry
  - Imaging
- QUANTIFICATION AND STATISTICAL ANALYSIS
  - Simulations
  - Flow data analysis
  - Image analysis

SUPPLEMENTAL INFORMATION

Supplemental information can be found online at https://doi.org/10.1016/j.celrep.2022.111118.

ACKNOWLEDGMENTS

We would like to thank members of the Cohen lab for many helpful discussions and funding from NIH R01 GM140711 and R01 GM092910.

AUTHOR CONTRIBUTIONS

Conceptualization, K.L. and B.C.; formal analysis, K.L.; investigation, K.L. and Y.W.; resources, M.V.S.; writing – original draft, K.L.; writing – review and editing, K.L. and B.C.; supervision, M.V.S. and B.C.; funding acquisition, B.C.

DECLARATION OF INTERESTS

The authors declare no competing interests.

Received: September 8, 2021
Revised: January 18, 2022
Accepted: June 28, 2022
Published: July 19, 2022

REFERENCES

Ahmad, K., and Henikoff, S. (2001). Modulation of a transcription factor counteracts heterochromatic gene silencing in Drosophila. Cell *104*, 839–847.

Anderson, C., Reiss, I., Zhou, C., Cho, A., Siddiqi, H., Mormann, B., Avelis, C.M., Deford, P., Bergland, A., Roberts, E., and Johnston, R.J. (2017). Natural variation in stochastic photoreceptor specification and color preference in Drosophila. Elife *6*, e29593.

Balázsi, G., van Oudenaarden, A., and Collins, J.J. (2011). Cellular decision making and biological noise: from microbes to mammals. Cell *144*, 910–925.

Bell, M.L., Earl, J.B., and Britt, S.G. (2007). Two types of Drosophila R7 photoreceptor cells are arranged randomly: a model for stochastic cell-fate determination. J. Comp. Neurol. *502*, 75–85.

Blake, W.J., Kærn, M., Cantor, C.R., and Collins, J.J. (2003). Noise in eukaryotic gene expression. Nature *422*, 633–637.

Blau, J., Xiao, H., McCracken, S., O'Hare, P., Greenblatt, J., and Bentley, D. (1996). Three functional classes of transcriptional activation domain. Mol. Cell. Biol. *16*, 2044–2055.

Brown, S.A., Weirich, C.S., Newton, E.M., and Kingston, R.E. (1998). Transcriptional activation domains stimulate initiation and elongation at different times and via different residues. EMBO J. *17*, 3146–3154.

Chang, H.H., Hemberg, M., Barahona, M., Ingber, D.E., and Huang, S. (2008). Transcriptome-wide noise controls lineage choice in mammalian progenitor cells. Nature *453*, 544–547.

Chubb, J.R., and Liverpool, T.B. (2010). Bursts and pulses: insights from single cell studies into transcriptional mechanisms. Curr. Opin. Genet. Dev. *20*, 478–484.

Cross, M.A., and Enver, T. (1997). The lineage commitment of haemopoietic progenitor cells. Curr. Opin. Genet. Dev. *7*, 609–613.

Dar, R.D., Hosmane, N.N., Arkin, M.R., Siliciano, R.F., and Weinberger, L.S. (2014). Screening for noise in gene expression identifies drug synergies. Science *344*, 1392–1396.

Dar, R.D., Razooky, B.S., Singh, A., Trimeloni, T.V., McCollum, J.M., Cox, C.D., Simpson, M.L., and Weinberger, L.S. (2012). Transcriptional burst frequency and burst size are equally modulated across the human genome. Proc. Natl. Acad. Sci. USA *109*, 17454–17459.

Dar, R.D., Shaffer, S.M., Singh, A., Razooky, B.S., Simpson, M.L., Raj, A., and Weinberger, L.S. (2016). Transcriptional bursting explains the noise–versus–mean relationship in mRNA and protein levels. PLoS One *11*, e0158298.

Dingemanse, M.A., de Boer, P.A., Moorman, A.F., Charles, R., and Lamers, W.H. (1994). The expression of liver-specific genes within rat embryonic hepatocytes is a discontinuous process. Differentiation *56*, 153–162.

Duarte, F.M., Fuda, N.J., Mahat, D.B., Core, L.J., Guertin, M.J., and Lis, J.T. (2016). Transcription factors GAF and HSF act at distinct regulatory steps to modulate stress-induced gene activation. Genes Dev. *30*, 1731–1746.

Elowitz, M.B., Levine, A.J., Siggia, E.D., and Swain, P.S. (2002). Stochastic gene expression in a single cell. Science *297*, 1183–1186.

Enver, T., Pera, M., Peterson, C., and Andrews, P.W. (2009). Stem cell states, fates, and the rules of attraction. Cell Stem Cell *4*, 387–397.

Fiering, S., Northrop, J.P., Nolan, G.P., Mattila, P.S., Crabtree, G.R., and Herzenberg, L.A. (1990). Single cell assay of a transcription factor reveals a threshold in transcription activated by signals emanating from the T-cell antigen receptor. Genes Dev. *4*, 1823–1834.

Gandrillon, O., Kolesnik-Antoine, D., Kupiec, J.J., and Beslon, G. (2012). Chance at the heart of the cell. Prog. Biophys. Mol. Biol. *110*, 1–4.

Gillespie, D.T. (1976). A general method for numerically simulating the stochastic time evolution of coupled chemical reactions. J. Comput. Phys. *22*, 403–434.

Golding, I. (2011). Decision making in living cells: lessons from a simple system. Annu. Rev. Biophys. *40*, 63–80.

Golding, I., Paulsson, J., Zawilski, S.M., and Cox, E.C. (2005). Real-time kinetics of gene activity in individual bacteria. Cell *123*, 1025–1036.

Govind, C.K., Yoon, S., Qiu, H., Govind, S., and Hinnebusch, A.G. (2005). Simultaneous recruitment of coactivators by Gcn4p stimulates multiple steps of transcription in vivo. Mol. Cell. Biol. *25*, 5626–5638.

Graf, T., and Enver, T. (2009). Forcing cells to change lineages. Nature *462*, 587–594.

Bahar Halpern, K., Tanami, S., Landen, S., Chapal, M., Szlak, L., Hutzler, A., Nizhberg, A., and Itzkovitz, S. (2015). Bursty gene expression in the intact mammalian liver. Mol. Cell *58*, 147–156.

Hansen, A.S., Amitai, A., Cattoglio, C., Tjian, R., and Darzacq, X. (2020). Guided nuclear exploration increases CTCF target search efficiency. Nat. Chem. Biol. *16*, 257–266.

Harris, L.A., Hogg, J.S., Tapia, J.J., Sekar, J.A.P., Gupta, S., Korsunsky, I., Arora, A., Barua, D., Sheehan, R.P., and Faeder, J.R. (2016). BioNetGen 2.2: advances in rule-based modeling. Bioinformatics *32*, 3366–3368.

Hensel, Z., Feng, H., Han, B., Hatem, C., Wang, J., and Xiao, J. (2012). Stochastic expression dynamics of a transcription factor revealed by single-molecule noise analysis. Nat. Struct. Mol. Biol. *19*, 797–802.

Kafri, P., Hasenson, S.E., Kanter, I., Sheinberger, J., Kinor, N., Yunger, S., and Shav-Tal, Y. (2016). Quantifying β-catenin subcellular dynamics and cyclin D1 mRNA transcription during Wnt signaling in single living cells. Elife *5*, e16748.

Kalo, A., Kanter, I., Shraga, A., Sheinberger, J., Tzemach, H., Kinor, N., Singer, R.H., Lionnet, T., and Shav-Tal, Y. (2015). Cellular levels of signaling factors are sensed by β-actin alleles to modulate transcriptional pulse intensity. Cell Rep. *13*, 1284–1285.

Kepler, T.B., and Elston, T.C. (2001). Stochasticity in transcriptional regulation: origins, consequences, and mathematical representations. Biophys. J. *81*, 3116–3136.

Liu, Z., and Tjian, R. (2018). Visualizing transcription factor dynamics in living cells. J. Cell Biol. *217*, 1181–1191.

Losick, R., and Desplan, C. (2008). Stochasticity and cell fate. Science *320*, 65–68.

McIsaac, R.S., Oakes, B.L., Wang, X., Dummit, K.A., Botstein, D., and Noyes, M.B. (2013). Synthetic gene expression perturbation systems with rapid, tunable, single-gene specificity in yeast. Nucleic Acids Res. *41*, e57.

Miller, A.C., Seymour, H., King, C., and Herman, T.G. (2008). Loss of seven-up from Drosophila R1/R6 photoreceptors reveals a stochastic fate choice that is normally biased by Notch. Development *135*, 707–715.

Munsky, B., Neuert, G., and Van Oudenaarden, A. (2012). Using gene expression noise to understand gene regulation. Science *336*, 183–187.

Näär, A.M., Lemon, B.D., and Tjian, R. (2001). Transcriptional coactivator complexes. Annu. Rev. Biochem. *70*, 475–501.

Normanno, D., Boudarène, L., Dugast-Darzacq, C., Chen, J., Richter, C., Proux, F., Bénichou, O., Voituriez, R., Darzacq, X., and Dahan, M. (2015). Probing the target search of DNA-binding proteins in mammalian cells using TetR as model searcher. Nat. Commun. *6*, 7357.

Ozbudak, E.M., Thattai, M., Kurtser, I., Grossman, A.D., and Van Oudenaarden, A. (2002). Regulation of noise in the expression of a single gene. Nat. Genet. *31*, 69–73.

Parab, L., Pal, S., and Dhar, R. (2021). Transcription factor binding activity is the primary driver of noise in gene expression. Preprint at bioRxiv. https://doi.org/10.1101/2020.07.27.222596.

Paré, A., Lemons, D., Kosman, D., Beaver, W., Freund, Y., and McGinnis, W. (2009). Visualization of individual Scr mRNAs during Drosophila embryogenesis yields evidence for transcriptional bursting. Curr. Biol. *19*, 2037–2042.

Pelet, S., Rudolf, F., Nadal-Ribelles, M., de Nadal, E., Posas, F., and Peter, M. (2011). Transient activation of the HOG MAPK pathway regulates bimodal gene expression. Science *332*, 732–735.

Pina, C., Fugazza, C., Tipping, A.J., Brown, J., Soneji, S., Teles, J., Peterson, C., and Enver, T. (2012). Inferring rules of lineage commitment in haematopoiesis. Nat. Cell Biol. *14*, 287–294.

Raj, A., and Van Oudenaarden, A. (2008). Nature, nurture, or chance: stochastic gene expression and its consequences. Cell *135*, 216–226.

Raj, A., Peskin, C.S., Tranchina, D., Vargas, D.Y., and Tyagi, S. (2006). Stochastic mRNA synthesis in mammalian cells. PLoS Biol. *4*, e309.

Raser, J.M., and O'Shea, E.K. (2004). Control of stochasticity in eukaryotic gene expression. Science *304*, 1811–1814.

Razooky, B.S., Pai, A., Aull, K., Rouzine, I.M., and Weinberger, L.S. (2015). A hardwired HIV latency program. Cell *160*, 990–1001.

Rodriguez, J., Ren, G., Day, C.R., Zhao, K., Chow, C.C., and Larson, D.R. (2019). Intrinsic dynamics of a human gene reveal the basis of expression heterogeneity. Cell *176*, 213–226.e18.

Rouzine, I.M., Weinberger, A.D., and Weinberger, L.S. (2015). An evolutionary role for HIV latency in enhancing viral transmission. Cell *160*, 1002–1012.

Sanchez, A., and Golding, I. (2013). Genetic determinants and cellular constraints in noisy gene expression. Science *342*, 1188–1193.

Scholes, C., DePace, A.H., and Sánchez, Á. (2017). Combinatorial gene regulation through kinetic control of the transcription cycle. Cell Syst. *4*, 97–108.e9.

Schwall, C.P., Loman, T.E., Martins, B.M.C., Cortijo, S., Villava, C., Kusmartsev, V., Livesey, T., Saez, T., and Locke, J.C. (2021). Tunable phenotypic variability through an autoregulatory alternative sigma factor circuit. Mol. Syst. Biol. *17*, e9832.

Senecal, A., Munsky, B., Proux, F., Ly, N., Braye, F.E., Zimmer, C., Mueller, F., and Darzacq, X. (2014). Transcription factors modulate c-Fos transcriptional bursts. Cell Rep. *8*, 75–83.

Shahrezaei, V., and Swain, P.S. (2008a). Analytical distributions for stochastic gene expression. Proc. Natl. Acad. Sci. USA *105*, 17256–17261.

Shahrezaei, V., and Swain, P.S. (2008b). The stochastic nature of biochemical networks. Curr. Opin. Biotechnol. *19*, 369–374.

Sherman, M.S., and Cohen, B.A. (2014). A computational framework for analyzing stochasticity in gene expression. PLoS Comput. Biol. *10*, e1003596.

Singh, A., and Weinberger, L.S. (2009). Stochastic gene expression as a molecular switch for viral latency. Curr. Opin. Microbiol. *12*, 460–466.

Singh, A., Razooky, B., Cox, C.D., Simpson, M.L., and Weinberger, L.S. (2010). Transcriptional bursting from the HIV-1 promoter is a significant source of stochastic noise in HIV-1 gene expression. Biophys. J. *98*, L32–L34.

Staller, M.V., Holehouse, A.S., Swain-Lenz, D., Das, R.K., Pappu, R.V., and Cohen, B.A. (2018). A high-throughput mutational scan of an intrinsically disordered acidic transcriptional activation domain. Cell Syst. *6*, 444–455.e6.

Stampfel, G., Kazmar, T., Frank, O., Wienerroither, S., Reiter, F., and Stark, A. (2015). Transcriptional regulators form diverse groups with context-dependent regulatory functions. Nature *528*, 147–151.

St-Pierre, F., and Endy, D. (2008). Determination of cell fate selection during phage lambda infection. Proc. Natl. Acad. Sci. USA *105*, 20705–20710.

Swain, P.S., Elowitz, M.B., and Siggia, E.D. (2002). Intrinsic and extrinsic contributions to stochasticity in gene expression. Proc. Natl. Acad. Sci. USA *99*, 12795–12800.

Symmons, O., and Raj, A. (2016). What's luck got to do with it: single cells, multiple fates, and biological nondeterminism. Mol. Cell *62*, 788–802.

Tan, D., Chen, R., Mo, Y., Gu, S., Ma, J., Xu, W., Lu, X., He, H., Jiang, F., Fan, W., and Huang, W. (2021). Quantitative control of noise in mammalian gene expression by dynamic histone regulation. Elife *10*, e65654.

Tantale, K., Mueller, F., Kozulic-Pirher, A., Lesne, A., Victor, J.M., Robert, M.C., Capozi, S., Chouaib, R., Bäcker, V., Mateos-Langerak, J., and Bertrand, E. (2016). A single-molecule view of transcription reveals convoys of RNA polymerases and multi-scale bursting. Nat. Commun. *7*, 12248.

Tiberi, S., Walsh, M., Cavallaro, M., Hebenstreit, D., and Finkenstädt, B. (2018). Bayesian inference on stochastic gene transcription from flow cytometry data. Bioinformatics *34*, i647–i655.

Vallania, F.L.M., Sherman, M., Goodwin, Z., Mogno, I., Cohen, B.A., and Mitra, R.D. (2014). Origin and consequences of the relationship between protein mean and variance. PLoS One *9*, e102202.

van Roon, M.A., Aten, J.A., Van Oven, C.H., Charles, R., and Lamers, W.H. (1989). The initiation of hepatocyte-specific gene expression within embryonic hepatocytes is a stochastic event. Dev. Biol. *136*, 508–516.

Walters, M.C., Fiering, S., Eidemiller, J., Magis, W., Groudine, M., and Martin, D.I. (1995). Enhancers increase the probability but not the level of gene expression. Proc. Natl. Acad. Sci. USA *92*, 7125–7129.

Waymack, R., Fletcher, A., Enciso, G., and Wunderlich, Z. (2020). Shadow enhancers can suppress input transcription factor noise through distinct regulatory logic. ELife *9*, e59351.

Weinberger, L.S., Burnett, J.C., Toettcher, J.E., Arkin, A.P., and Schaffer, D.V. (2005). Stochastic gene expression in a lentiviral positive-feedback loop: HIV-1 Tat fluctuations drive phenotypic diversity. Cell *122*, 169–182.

Weinberger, L.S., Dar, R.D., and Simpson, M.L. (2008). Transient-mediated fate determination in a transcriptional circuit of HIV. Nat. Genet. *40*, 466–470.

Wolff, S.C., Kedziora, K.M., Dumitru, R., Dungee, C.D., Zikry, T.M., Beltran, A.S., Haggerty, R.A., Cheng, J., Redick, M.A., and Purvis, J.E. (2018). Inheritance of OCT 4 predetermines fate choice in human embryonic stem cells. Mol. Syst. Biol. *14*, e8140.

Zeng, L., Skinner, S.O., Zong, C., Sippy, J., Feiss, M., and Golding, I. (2010). Decision making at a subcellular level determines the outcome of bacteriophage infection. Cell *141*, 682–691.

Zenklusen, D., Larson, D.R., and Singer, R.H. (2008). Single-RNA counting reveals alternative modes of gene expression in yeast. Nat. Struct. Mol. Biol. *15*, 1263–1271.

Zhang, Z., English, B.P., Grimm, J.B., Kazane, S.A., Hu, W., Tsai, A., Inouye, C., You, C., Piehler, J., Schultz, P.G., and Tjian, R. (2016). Rapid dynamics of general transcription factor TFIIB binding during preinitiation complex assembly revealed by single-molecule analysis. Genes Dev. *30*, 2106–2118.

Zoller, B., Nicolas, D., Molina, N., and Naef, F. (2015). Structure of silent transcription intervals and noise characteristics of mammalian genes. Mol. Syst. Biol. *11*, 823.

STAR★METHODS

KEY RESOURCES TABLE

REAGENT or RESOURCE	SOURCE	IDENTIFIER
Chemicals, peptides, and recombinant proteins		
β-estradiol	Sigma	E2758
Experimental models: Organisms/strains		
Yeast:FY4:*MAT*a prototroph	Fred Winston	(S288c)
Yeast:FY5:MATalpha prototroph	Fred Winston	(S288c)
Yeast:GCN4 mutant library:*MATa*/MATalpha, synthetic TF-Kan^{r}::*ura3*/*URA3* GFP reporter-nat^{R}::YBR032w/YBR032w	Max Staller	N/A
Yeast:VP16:*MATa*/MATalpha, synthetic TF-Kan^{r}::*ura3*/*URA3* GFP reporter-nat^{R}::YBR032w/YBR032w	Max Staller	MY447, MY448
Yeast:GCN4 WT:*MATa*/MATalpha, synthetic TF-Kan^{r}::*ura3*/*URA3* GFP reporter-nat^{R}::YBR032w/YBR032w	Max Staller	MY449, MY450, MY461, MY457
Yeast:War1:*MATa*/MATalpha, synthetic TF-Kan^{r}::*ura3*/*URA3* GFP reporter-nat^{R}::YBR032w/YBR032w	Max Staller	YM23.23, YM23.24, YM23.31, YM23.32
Yeast:Gal4:*MATa*/MATalpha, synthetic TF-Kan^{r}::*ura3*/*URA3* GFP reporter-nat^{R}::YBR032w/YBR032w	Max Staller	MY459, MY460
Yeast:No AD:*MATa*/MATalpha, synthetic TF-Kan^{r}::*ura3*/*URA3* GFP reporter-nat^{R}::YBR032w/YBR032w	Max Staller	MY445, MY446, MY458
Oligonucleotides		
See supplemental information	IDT	N/A
Recombinant DNA		
See Table S2	Synbio Tech	S014756
Software and algorithms		
BioNetGet	Harris et al., 2016	https://bionetgen.org/
Jupyter Notebook	https://jupyter.org/	https://jupyter.org/

RESOURCE AVAILABILITY

Lead contact

Please direct any requests for further information or reagents to the lead contact, Barak Cohen (cohen@wustl.edu).

Materials availability

Plasmids and yeast strains generated in this study are available upon request from the lead contact.

Data and code availability

- Data and code generated in this study are available upon request from the lead contact.
- This paper does not report original code.
- Any additional information required to reanalyze the data reported in this paper is available from the lead contact upon request.

EXPERIMENTAL MODEL AND SUBJECT DETAILS

Yeast strains

We repurposed the yeast strains created by Staller et al. (Staller et al., 2018). These strains (*MATa*/MATalpha, synthetic TF-Kan^{r}::*ura3*/*URA3* GFP reporter-nat^{R}::YBR032w/YBR032w) are generated from crosses between derivatives of FY4 (*MATa*, synthetic

TF-Kan^r::*ura3*) and FY5 (MATalpha, GFP reporter-nat^R::YBR032w). Each synthetic TF construct consists of an mCherry tag, a murine Zif268 DNA binding domain (DBD), a human estrogen response domain (ERD), and an activation domain (AD), driven by the yeast ACT1 promoter. The activation domains were either sampled from the library of GCN4 mutants described in Staller et al. by picking clones at random, or derived from wild type ADs (Table S2). Sequence files of the all wild-type synthetic TF-AD fusions are available in supplementary folder 1. The GFP reporter is the same as reported in Staller et al. and consists of a fast maturing GFP variant, with expression driven by six upstream Zif268 binding sites and the P3 promoter.

Culture conditions

All strains were obtained from frozen glycerol stocks. For the experiments involving wild-type activation domains, cultures were seeded by pipetting 2 uL of each strain onto a YPD agar plate, streaking out, and growing for 2 days in a 30 degree incubator. For each experiment, individual colonies were then picked from the plates and grown out overnight in tubes containing 3 mL of SC dextrose medium. These tubes were constantly rotated on a wheel in a 30 degree incubator throughout the growth process. The optical densities of 1:10 dilutions of the overnight cultures were then measured, and all cultures were diluted to an OD of 0.0225. For each combination of strain and level of induction, 200 uL of diluted culture was added to a well of a deep 96 well plate. 50 uL of diluted beta-estradiol was then added to the well (final concentrations are listed in Table S1). The diluted cultures were incubated with the beta-estradiol in a shaker incubator set to 300 rpm for 5 h before measuring.

For the experiments involving mutant activation domains, the initial cultures were seeded by pinning from the 96 well plate containing the glycerol stocks onto a YPD agar plate. Liquid cultures were then seeded by pinning from the agar cultures into a deep well plate with 300 uL of SC in each well. The deep well plate was agitated in a shaker incubator overnight.

METHOD DETAILS

Molecular cloning and transformations

To generate the remaining yeast strains not described in Staller et al. (*MATa*/MATalpha, synthetic TF-Kan^r::*ura3*/*URA3* GFP reporter-nat^R::YBR032w/YBR032w), eleven AD sequences (Table S2) were ordered as DNA fragments from SynBio Technologies (Monmouth Junction, NJ). Those AD fragments have homology arms for cloning into pMV219 (Addgene), a plasmid vector that contains the pACT1-mCherry-DBD-ERD cassette described above. More specifically, pMV219 was digested with Nhe1-HF (NEB, R3131S) and Asc1-HF (NEB,R0558S), AD sequences were cloned downstream of the ERD using HIFI assembly (NEB, E2621S). The entire pACT1-mCherry-DBD-ERD-AD region was then PCR amplified using primers YP16 and YP17 (supplemental information) with homology targeting the URA3 locus. The PCR product was then transformed into FY4 S288c yeast by incubating with a mixture of 30–33% PEG, 100 uM lithium acetate, and 0.3 mg/mL boiled salmon sperm DNA for 30 min at 30 C followed by 1 h of heat shock at 42 C. The transformed yeast were spun down, resuspended in YPD, and plated on nonselective medium, followed by replica plating onto YPD+G418 plates (200 mg/mL). The KanR positive yeast were then struck out onto SC-URA and 5-FOA (1 mg/mL) plates to test for loss of the URA3 locus.

Integrations were confirmed by colony PCR targeting the upstream breakpoint. To extract genomic DNA, URA- yeast strains were grown overnight in YPD, spun down and resuspended in 500 ul each of lysis buffer containing 100 mM Tris, 50 mM EDTA, and 1% SDS. They were then vortexed with silica beads for 2 min each. The liquid was then pipetted off the beads, mixed with 275 uL of 7M ammonium acetate pH7, and incubated for 5 min 65 C then 5 min on ice. 500 uL of chloroform was added, and the mixture was vortexed and spun for 2 min. The supernatant was then added to 1 mL isopropanol, incubated for 5 min at room temperature, and spun down for 5 min. The resulting pellet was then washed with 70% ethanol, air dried, and dissolved. For PCR, the genomic DNA was first digested with Nhe1. 2.5 uL of digest was then mixed with 2.5 uL of each primer (put sequences in supplemental information), 2.5 uL water, and 10 uL of NEB OneTaq and run for 34 cycles of 30 s at 94 C, 30 s at 55 C, and 1 min at 72 C. The resulting PCR product was loaded directly onto an agarose gel, which was then run and imaged.

Beta-estradiol induction and flow cytometry

All single-cell fluorescence measurements were collected using a Beckman Coulter cytoflex S flow cytometer.

In the experiments with wild-type activation domains, the optical densities of 1:10 dilutions of the overnight cultures were first measured, and all cultures were diluted to an OD of 0.0225. For each combination of strain and level of induction, 200 uL of diluted culture was added to a well of a deep 96 well plate. 50 uL of diluted beta-estradiol was then added to the well (final concentrations are listed in Table S1). The diluted cultures were incubated with the beta-estradiol in a shaker incubator set to 300 rpm for 5 h before measuring. Finally, 100,000 such single-cell fluorescences were collected for each combination of activation domain and induction level.

In the experiments with mutant activation domains, 5 uL of overnight culture from each well was first diluted into 200 uL of SC in the corresponding well of a new deep well plate. 50 uL of 1 mM beta-estradiol diluted 1:1000 was added to each well of the new plate, and the plate was again incubated for 5 h in a shaker set to 300 rpm before measuring. Strains for which we suspected contamination or other experimental error were then subjected to verification experiments. These involved growing them up as liquid cultures in tubes and then streaking them out on agar plates. Single colonies were then picked and used to start liquid cultures which were then induced and measured using the same protocols used for the wild-type activation domains, except that, for each mutant, we collected measurements for a fixed 45 s.

Imaging

Yeast strains MY447 (expressing a VP16 fusion), YM23.31 (expressing a War1 fusion), MY450 (expressing a GCN4 fusion), and MY460 (expressing a Gal4 fusion) were grown overnight from streakouts in 1 mL of SC. They were then incubated for 4 h in 250 uL of SC with or without 200 uM beta-estradiol. The yeast were immobilized on agarose pads and imaged on a Zeiss LSM 880 Confocal.

QUANTIFICATION AND STATISTICAL ANALYSIS

Simulations

Sets of simulations were run to predict the effects on mean and noise of varying one or two parameters in a given stochastic model of gene expression, while keeping all others constant. The models simulated were the random telegraph model (Shahrezaei and Swain, 2008a, 2008b; Sherman and Cohen., 2014; Tiberi et al., 2018), the multi-state model of Rodriguez el at (Rodruigez et al., 2019), the refractory period model of Zoller et al. (Zoller et al., 2015), and the transcription cycle model of Scholes et al. (Scholes et al., 2017). These simulations were run using the implementation of Gillespie's stochastic simulation algorithm (Gillespie, 1976) in BioNetGen (Harris et al., 2016). Model files are available in supplemental information, and sets of input parameters used for each simulation are available in Table S3. For each set of parameters, 1000 individual simulations were run and a mean and a Fano factor was computed for the distribution of protein expression at the ends of the individual runs. The relationships between mean and Fano factor over multiple sets of parameters within the same model were plotted using the Matplotlib and Seaborn packages in Python.

Flow data analysis

Outliers in forward and side scatter area and height were removed at the collection stage through gating. Summary statistics of GFP fluorescence (mean and Fano factor) were then computed over the cells whose mCherry fluorescence fell between 300 and 400 units, and the results were plotted, again using Matplotlib and Seaborn. To generate each plot, means and Fano factors were computed for each of 3 replicates (n = 3 for all figures), and scatterplots were made of means of the summary statistics, with the standard deviations of the summary statistics across replicates plotted as error bars.

Image analysis

The images were segmented in CellProfiler using the GFP signal, and total mCherry signal was quantified for the nuclear and cytoplasmic segments of each cell. Nuclear/cytoplasmic ratios were computed, and the distributions of these ratios across cells were plotted using Matplotlib and Seaborn.